B0912

Cyclic degradation analysis of reversible Solid Oxide Cell short-stack

Suhas Nuggehalli Sampathkumar (1, 2), Mar Pérez-Fortes (1), Stefan Diethelm (1), David Constantin (1), Philippe Aubin (1), Guillaume Jeanmonod (1), Jan Van herle (1), Bhaskar Reddy Sudireddy (2), Xiufu Sun (2), Karine Couturier (3), Stéphane Di Iorio (3), Pierre Hanoux (3)

(1) École Polytechnique Fédérale de Lausanne (EPFL), 1950 Sion, Switzerland.
(2) Technical University of Denmark (DTU), DK-2800 Kgs. Lyngby, Denmark.
(3) Univ. Grenoble Alpes – CEA/LITEN, 38054 Grenoble, France
Tel.: +41 21 693 59 68
suhas.nuggehallisampathkumar@epfl.ch

Abstract

The deployment of renewable energy systems has been increasing steadily in recent years. The intermittency associated with the renewable electricity supply can be addressed through the usage of energy storage and release systems. In this framework, reversible solid oxide cells (rSOC) integrated in power-to-gas-to-power systems can convert excess electricity into multiple useful fuels (solid oxide electrolysis (SOE) mode) and restitute it when its renewable production is too low (solid oxide fuel cell (SOFC) mode). To make rSOC competitive and durable, low degradation for the targeted lifetime must be achieved.

In BALANCE project (H2020 GA no:731224), with the purpose of assessing the degradation of rSOC in both modes, a cyclic durability test as shown in the graphical abstract was conducted on a 5-cell short stack (100 cm^2 active area each) designed by CEA, using H2-electrode supported Ni-YSZ cells manufactured by DTU. The composition of the inlet gases was H_2/N_2:50/50 in SOFC mode and H_2/H_2O:20/80 in SOE mode. Steady-state initial performance revealed an improvement for all the repeatable units (RUs) in SOFC mode. In SOE mode, only RU 4 and 5 showed enhanced performance while RU1-3 degraded. Afterwards, J-V characteristic curves showed loss of performances in both modes all along the experiment. A distribution of relaxation time analysis performed on the electrochemical impedance spectra measured regularly throughout the test revealed that the oxide ion transport through the H2-electrode and the O2-electrode is responsible for the observed degradation, over the 1400 h test duration.

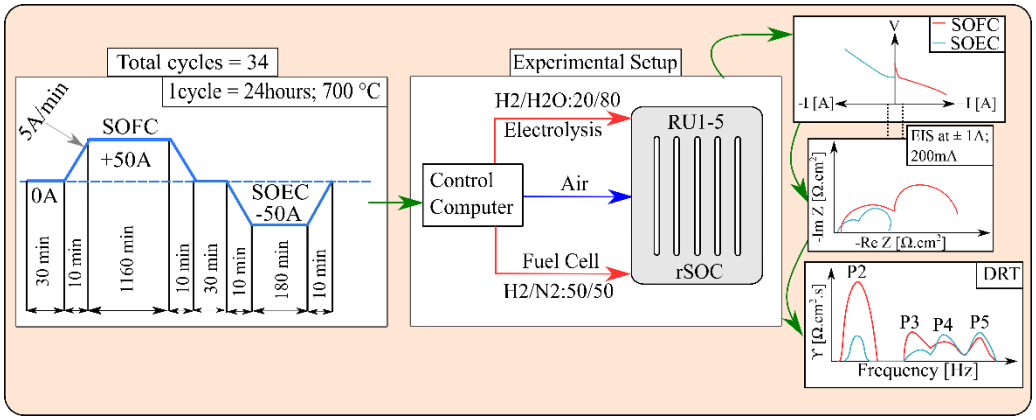

1 Introduction

As we progress through the 21st century, climate change has led to extreme weather, with heat and cold waves setting record temperatures in different parts of the world [1–4]. A major step towards limiting the global temperature rise to 1.5 °C is the Paris Climate Agreement [5]. The deal has called for countries to declare Nationally Determined Contributions (NDC) towards emission cuts [6]. In this frame, the implementation of renewable energy systems could be promoted in the national energy mix of technologies.

Due to intermittency of electricity production associated with the renewable sources, there is a strong requirement for the implementation of energy storage solutions. Energy storage systems have the potential to solve the demand and supply mismatch by transforming the excess of electricity during peak production and by discharging the stored energy during peak demand. A solution to the distribution of electricity, coupled with decarbonization, is the implementation of power-to-hydrogen-to-power systems [7]. The production of hydrogen is already mature and competitive with fossil fuels (mainly natural gas) at small and medium scales. The costs are set to drop further as the renewable electricity and electrolysis get cheaper [7,8].

The development of high efficiency reversible Solid Oxide Cells (rSOC) can offer a possible solution against curtailment of renewable electricity production. The excess electricity can be used to synthesize hydrogen. Various tests on rSOC stacks have been conducted to analyze efficiencies. For example, R. Peters et.al [9] performed long term tests on a 40-cell rSOC stack (4 x 10-cell stack) reaching a maximum fuel utilization of 97.3% in SOFC mode and steam conversion of 85% in SOE mode. 77 rapid switching cycles were performed revealing issues with the steam generation unit. The stack efficiencies improved with increasing fuel recirculation. Van Nhu Nguyen et. al [10] performed long-term steady-state degradation tests on a two-cell planar rSOC short stack with a lower fuel utilization of 45% in SOFC mode (4000 h, 750°C, 0.5 A cm^{-2}, H_2:H_2O= 80:20) and 15% in SOE mode (2000h, 800°C, - 0.875 A cm^{-2}, H_2:H_2O = 1:1). The degradation was found to be 0.6 %kh^{-1} and ≈0 %kh^{-1} in the SOFC and SOE modes, respectively. A review article on rSOC by M.B. Mogensen et.al [11] revealed that the challenges faced by the rSOC systems were degradation due to mechanical failures, nickel agglomeration/migration on the H2-electrode, segregation in the O2-electrode, loss of contact and electrode poisoning.

Electrochemical impedance spectroscopy (EIS) is a non-destructive technique that is useful to study degradation in rSOC. EIS coupled with distribution of relaxation time (DRT) analysis helps to identify loss mechanisms and isolating the cause of degradation. There are no detailed degradation studies on rSOC for which DRT has been used. Since DRT is a comparative study, generally a sensitivity analysis is needed. However, as the composition of the cells used in this work were the same as reported in single cell tests done by Xiufu et.al [12,13], it is safe to carry out the analysis of DRT with the same assumptions on the peak attribution.

2 Experimental setup and methodology

In this study we investigated a H2-electrode supported (Ni-YSZ) 5-cell rSOC short stack, for an experimental duration of 1400 hours. The rSOC short stack was designed and produced by CEA with cells manufactured by DTU. The integrated cells were planar having 10x10 cm^2 active surface area each.

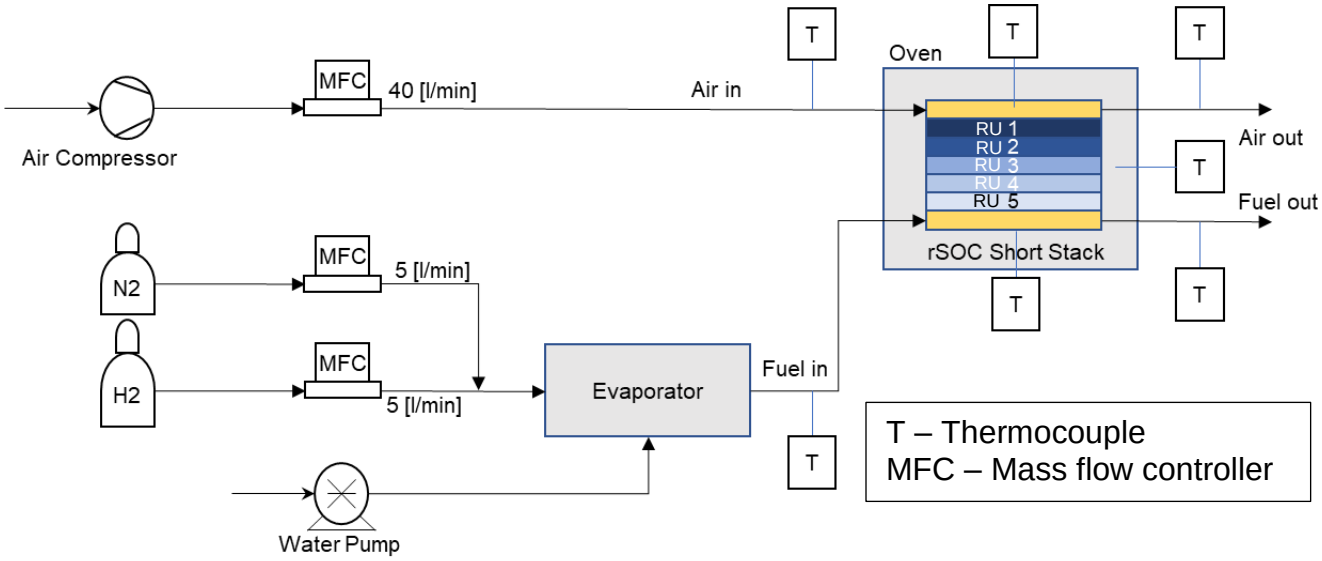

Figure 1: Schematic of the experimental setup used for rSOC test at EPFL.

The H2-electrode reactant composition was 50:50 N_2:H_2 in SOFC mode and 20:80 H_2:H_2O in SOE mode. The total reactant flow rate was 10 l min^{-1} in both modes. At the O2-electrode a compressed air flow of 40 l min^{-1} was fed to the rSOC stack. The rSOC short stack was placed in an oven that is maintained at 700°C as shown in Figure 1. Mass flow controllers were used to set the gas composition in both modes and a water pump to control the amount of water fed to the evaporator (EBZ Gmbh). Air and reactant flows were preheated to 700°C, which were verified by thermocouples at the inlets. The stack J-V characteristic and the EIS of each repeatable unit (RU) were measured every 7 to 8 cycles throughout the test. The EIS measurements were done at ±1A DC bias with 200 mA/1000 mA perturbation in SOFC/SOE modes.

3 Results and Discussion

The voltage of each RU is reported for the whole test duration in Figure 2. After the initial heat treatment of the rSOC short stack, initial J-V and EIS measurements were recorded, indicated as Step1 in Figure 2. The SOFC and SOE steady-state operations were performed with a bias of ±0.5 A/cm^2. The duration of the steady state operations was 80 hours in SOFC mode and 120 hours in SOEC mode. Those initial steps were followed by 24-hour cycling of the rSOC short stack with 19 hours 20 min in SOFC mode and 3 hours in SOE mode. The remaining time was the transient between the two modes. Due to data acquisition issues, some of the cycles appear to be missing as indicated. Overall, we performed 34 or 35 cycles during the test duration of almost 1400 hours.

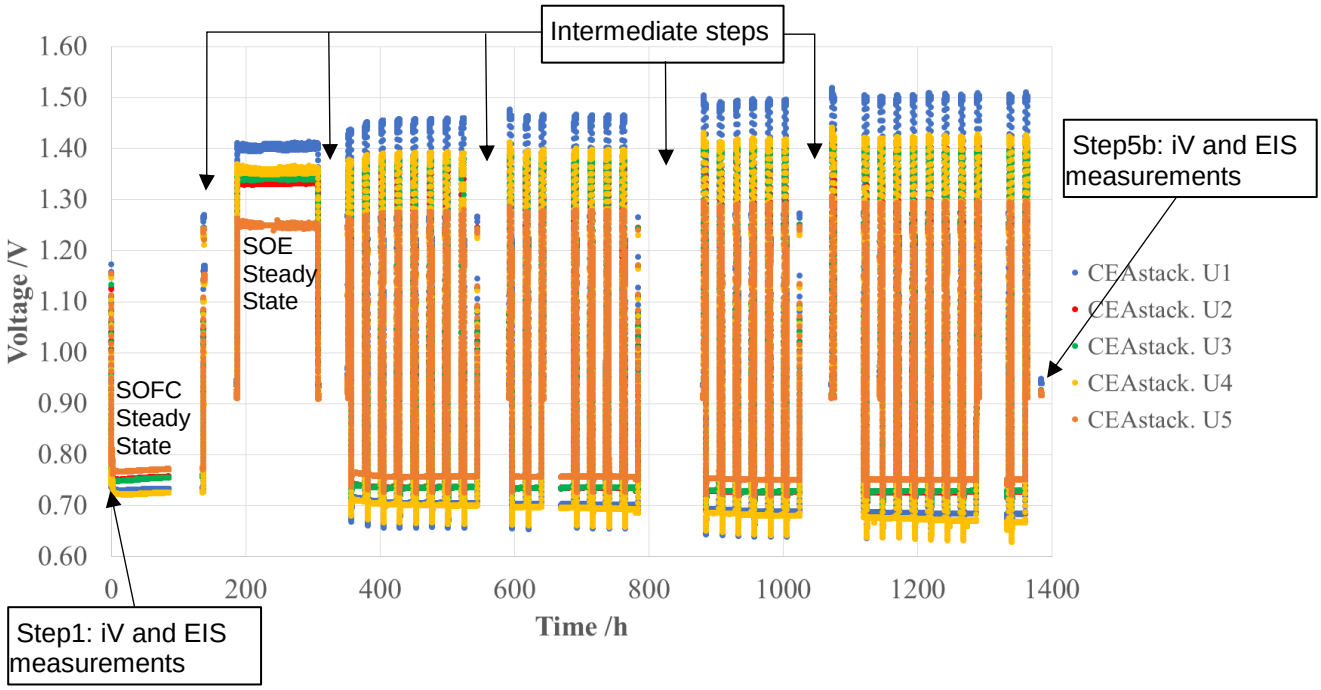

Figure 2: Voltage versus time characteristics of all the RU during the whole experiment

3.1. Steady-state degradation

The steady-state voltage degradation rates were calculated between 10-85 hours in the SOFC mode and 189-308 hours in the SOE mode. The rates revealed improvement of performance in the SOFC mode for all the RU as shown in Figure 3a. In the SOE mode, the rSOC showed degradation for RU1-3 while RU4-5 improved in performance as shown in

b. The voltage improvement in SOFC mode ranges from 40 mV kh^{-1} (8 % kh^{-1}) for RU4 up to 90 mVkh^{-1} (12.5 % kh^{-1}) for RU3. In SOE mode, RU1 has the highest degradation rate at 35 mV kh^{-1} (2.5 % kh^{-1}) while RU5 improves the most at -40 mV kh^{-1} (-3.4 % kh^{-1}). Negative degradation rates in SOE mode and positive in SOFC mode signify improvement in performance. As RU3 is the geometric center of the rSOC short-stack and had good performance in both modes, it will be investigated further.

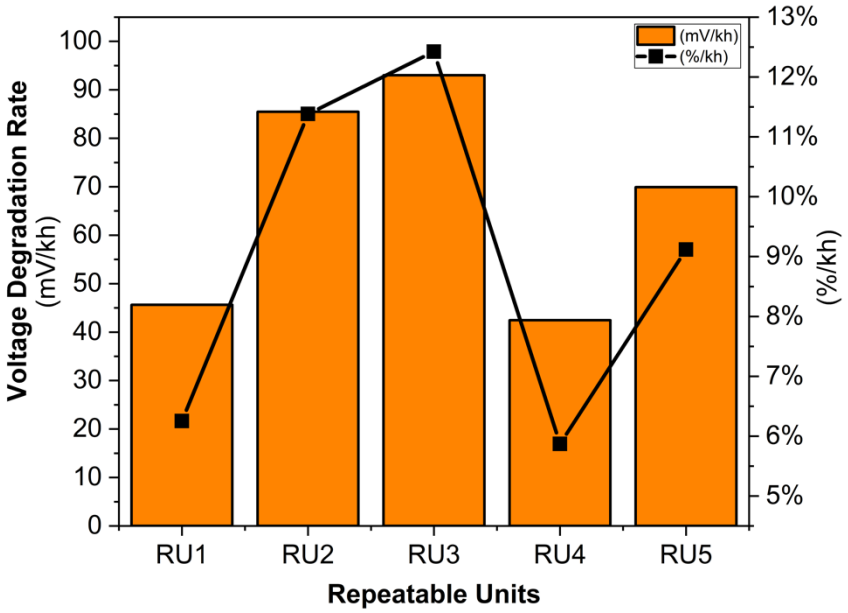

Figure 3a: Steady-state degradation rates in SOFC mode.

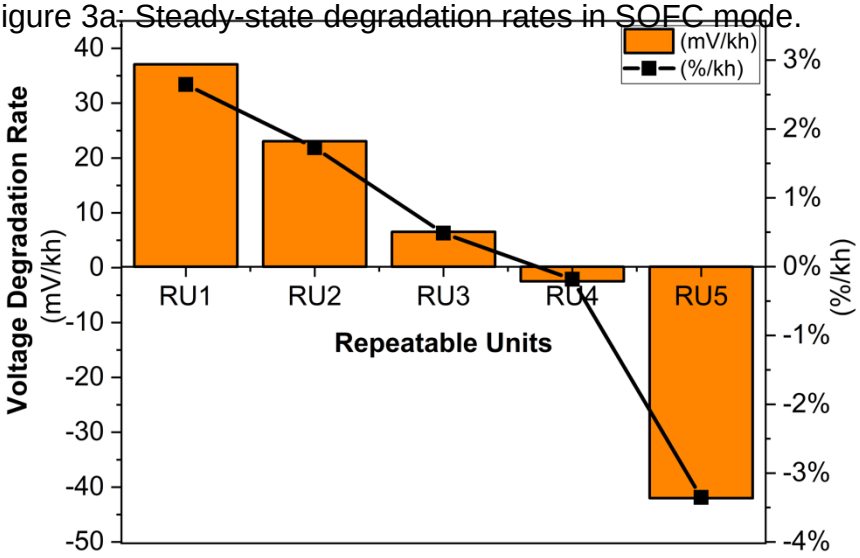

Figure 4b: Steady-state degradation rates in SOE mode.

3.2. SOFC/SOE J-V characteristics and EIS measurements

Degradation in a cell causes an increase in overpotentials at a fixed current density. The J-V characteristic curve for a fuel cell quantifies this rise in overpotential in terms of change in the area-specific resistance (ASR). The evolution of ASR and the open-circuit voltage (OCV) values determine the durability of a cell.

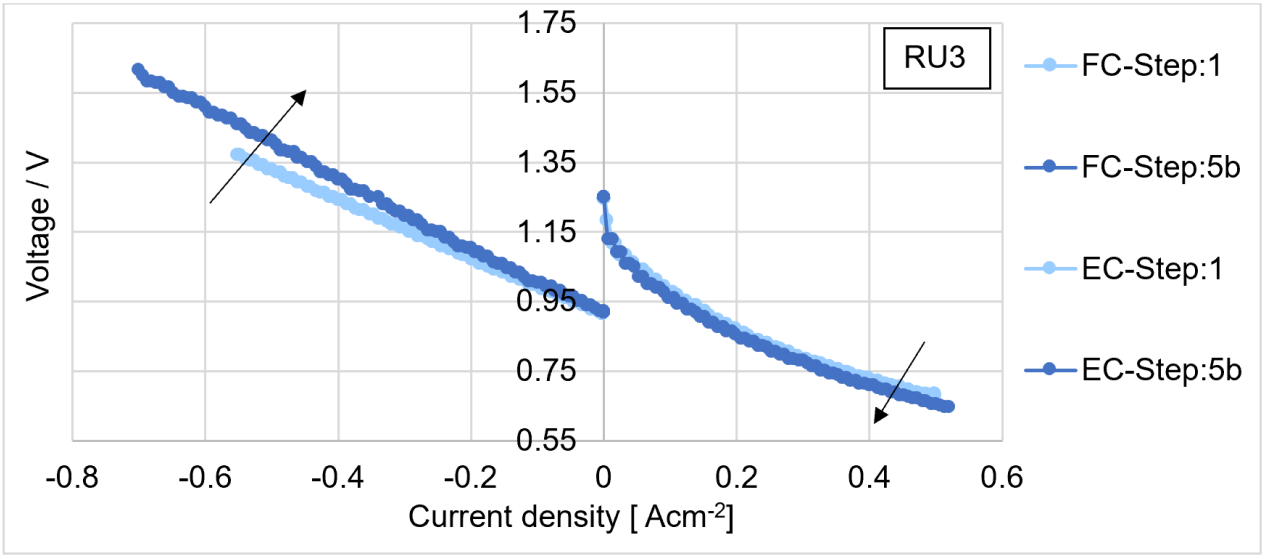

Figure 5: Current vs Voltage Characteristics of RU3 (representative of all the RU) at the beginning (Step 1) and end of the experiment (Step 5b)

The OCV in both modes for the rSOC short stack was nearly constant during the experiment as shown in Figure 4, indicating stable stack tightness and gas supply. Intermediate measurements were done to validate changes in the J-V characteristics and EIS measurement of the rSOC. The ASR $[\Omega.cm^2]$ was calculated using the slope of the J-V curve at 0.4 A cm^{-2} as shown in equation (1).

$$\text{ASR} = \left(\frac{U_{avg}}{J_{avg}}\right) \tag{1}$$

where $\left(\frac{U_{avg}}{J_{avg}}\right)$ is the slope of the J-V curve in the vicinity of 0.4 A cm^{-2} and U_{avg} [V] is the average voltage level corresponding to average current density values J_{avg} [A cm^{-2}]. The increase of ASR can be clearly seen in Figure 6 between step1 and step 5b in both modes, indicating degradation of RU3. Using equation **Error! Reference source not found.** and **Error! Reference source not found.**, the ASR and voltage degradation rates were calculated.

$$ASR\ Degradation\ rate = \frac{\Delta\text{ASR}(t)/ASR_o}{t} \times 100\ \times 1000 \tag{2}$$

$$Voltage\ Degradation\ rate = \frac{\Delta U(t)/U_o}{t} \times 100\ \times 1000 \tag{3}$$

where $\Delta ASR(t)$ is the change in ASR at 0.4 A cm^{-2} as a funtion of time – i.e. between step1 and steb5b; ASR_o is the initial ASR value at 0.4 A cm^{-2} in step1; $\Delta U(t)$ is the voltage change

value between step1 and step 5b; U_o is the voltage at 0.4 A cm^{-2} at step1 and $t = 1385\ h$ is the time duration between the step1 and step5b in h.

At the current density of 0.4 A cm^{-2}, the ASR degradation rate for SOFC and SOE modes were found to be 3.80 % kh^{-1} and 15.97 % kh^{-1} respectively. The corresponding voltage degradation rates for the SOFC and SOE modes were 1.07 % kh^{-1} and 3.60 % kh^{-1} respectively. The change in OCV for both modes was negligible.

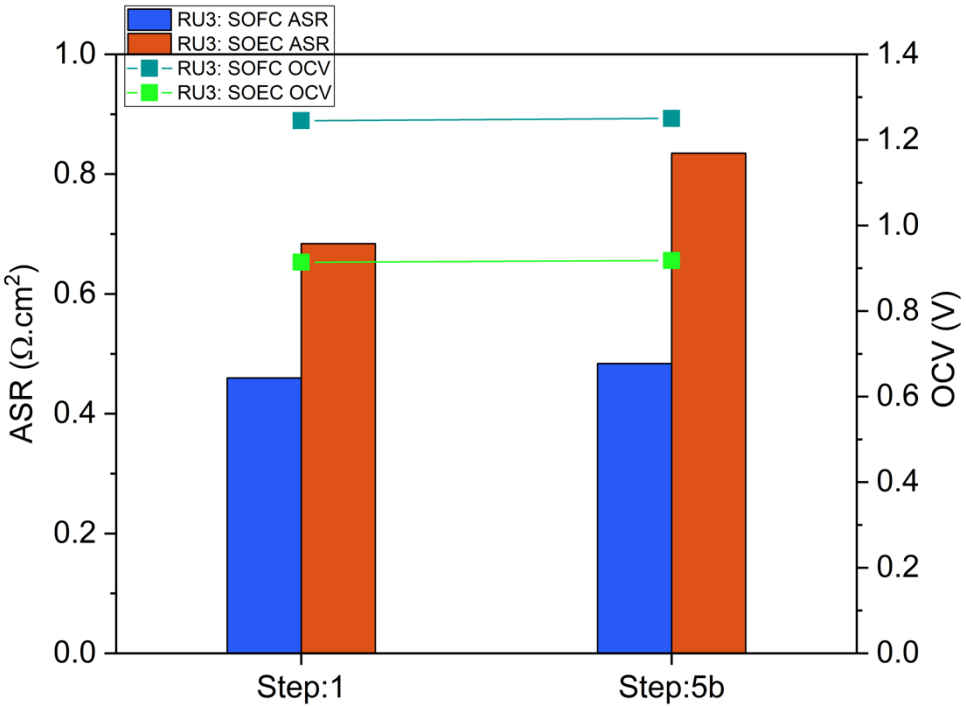

Figure 6: ASR (calculated at 0.4 A cm^{-2}) and OCV evolution of RU3 during the whole experiment.

EIS measurements help to quantify the change in ASR value. The EIS spectra are represented as a Nyquist plot in Figure 6 and Figure 8 from which the ohmic resistance R_{ohm} and total resistance R_{total} (ASR) were determined. The difference between R_{ohm} and R_{tot} gives the total polarization resistance R_{pol}. The ASR values between Figure 6 and the Nyquist plots are different as the EIS measurements were performed close to OCV (0.01 A cm^{-2}) and not at 0.4 A cm^{-2}.

As the EIS measurements were close to OCV, it can be seen from Figure 6 that for SOFC mode, between step1 and step5b, there's a small rise in R_{ohm} while a large change can be seen in R_{tot}, signifying an increase of the polarization resistance. This trend was also observed in SOE mode as shown in Figure 8. The quality of the EIS spectra were verified by performing Kramers Krönig tests. The EIS spectra for both modes were affected by noise due to steam generation at low frequencies and high frequency inductive effects. The spectra were trimmed, smoothed, corrected for inductive effects and extrapolated at higher frequencies to determine R_{ohm} [14].

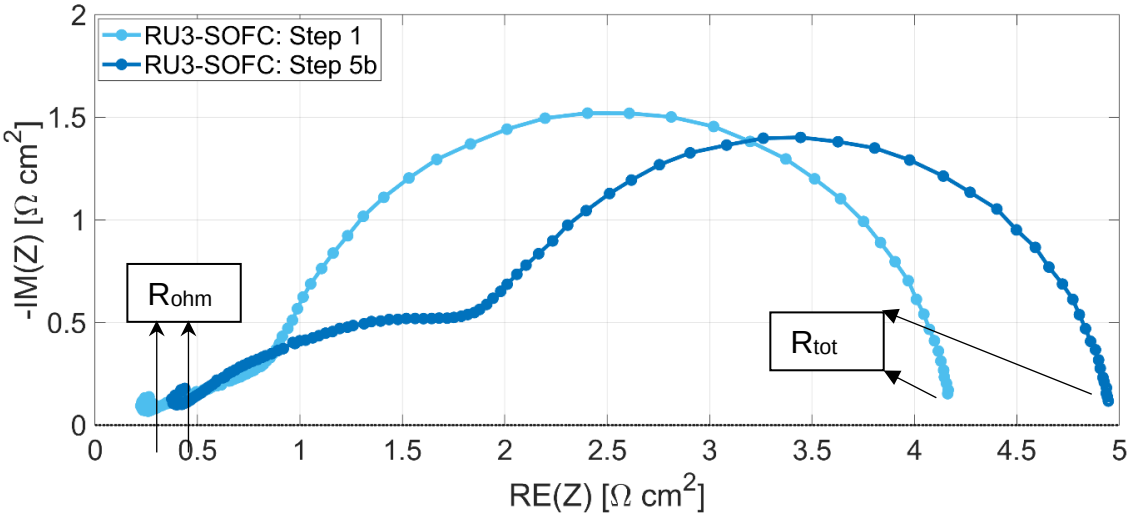

Figure 7: Nyquist plot corresponding to the EIS measurements for RU3 in SOFC mode at 700°C, +1A bias and 200mA perturbation.

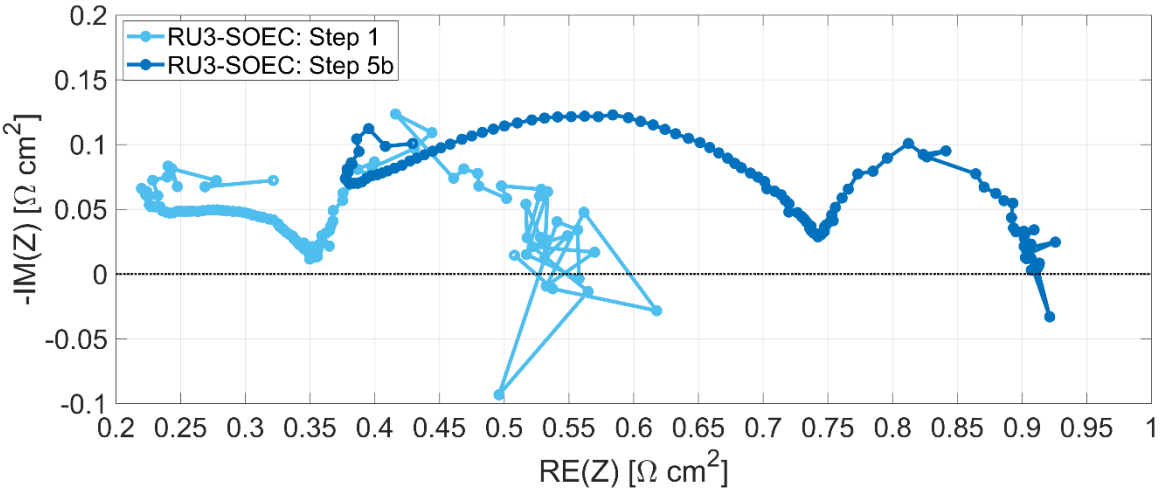

Figure 8: Nyquist plot corresponding to the EIS measurements for RU3 in SOE mode at 700°C, -1A bias and 1000mA perturbation.

3.3. Distribution of Relaxation Time (DRT) analysis in SOFC/SOE mode.

Table 1: DRT peak description and their respective range of frequencies, adapted from [12–14].

Peak no.	Peak range (Hz)	Peak Description
P1	10^{-1} - 10^{1}	Gas diffusion resistance peak.
P2	10^{1} -10^{2}	Oxygen-surface exchange and oxide ion transport resistance in the O2-electrode (LSC-CGO).
P3	10^{2} - 10^{3}	Charge transfer resistance peak attributed to H2- electrode (Ni-YSZ).
P4	> 10^{3}	Oxide Ion transfer resistance peak attributed to H2- electrode (Ni-YSZ).

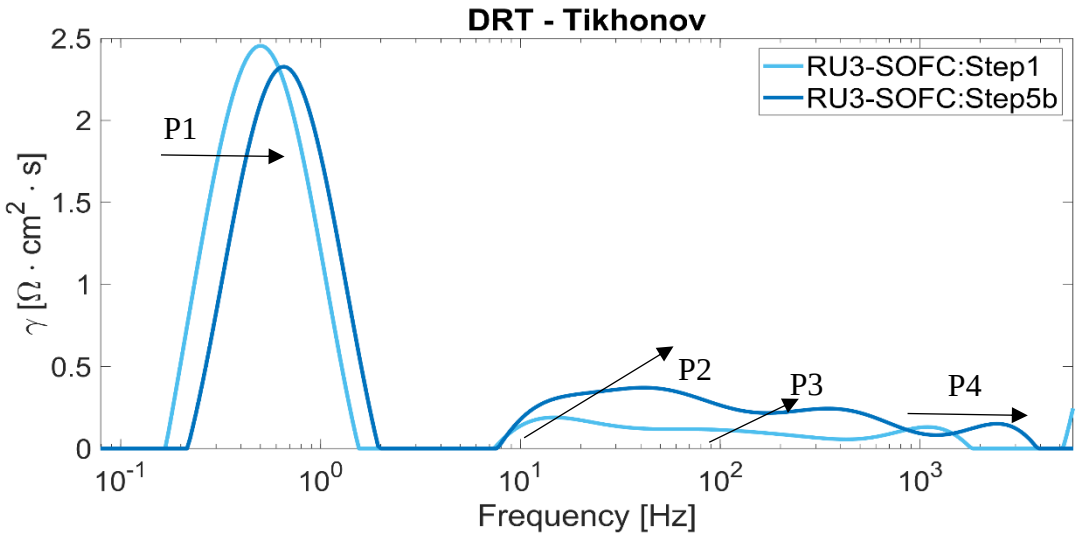

Figure 9: DRT plotted using Tikhonov regularization of RU3 EIS spectra in SOFC mode

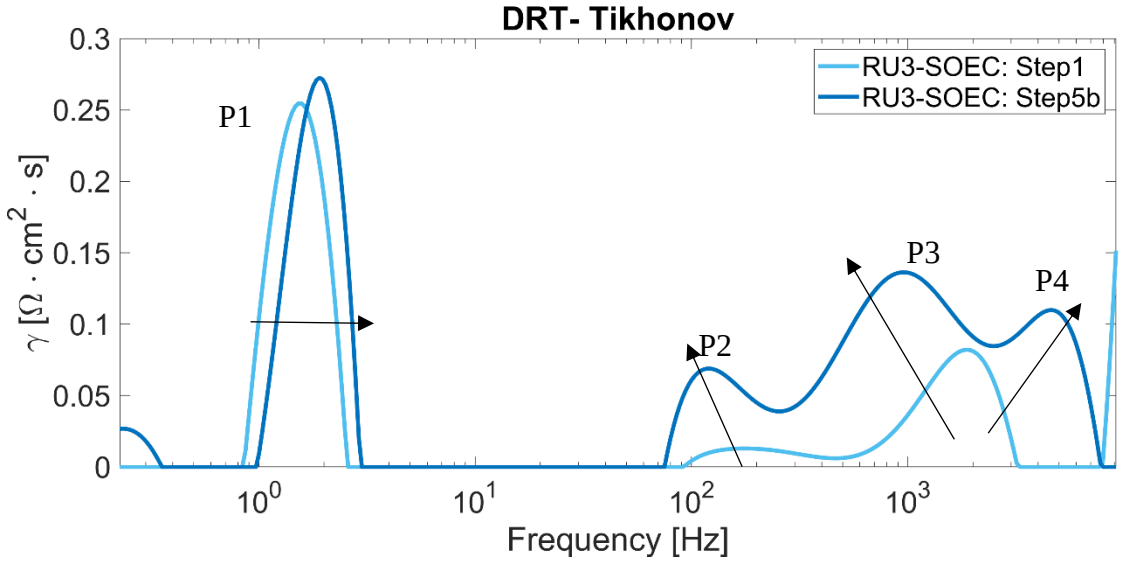

Figure 10: DRT plotted using Tikhonov regularization of RU3 EIS spectra in SOE mode

An EIS spectrum is a convolution of all the intrinsic mechanisms occurring in a rSOC. Here an attempt was made to deconvolute the EIS spectra using Tikhonov regularization. Further information on the methodology can be found in Caliandro P. et. al [14]. The resulting distribution of relaxation time (DRT) spectra are shown in Figure 8 and **Error! Reference source not found.** for the SOFC/SOE modes respectively. The peaks of the DRT corresponding to various processes adapted from [12–14] are shown in Table 1.

In both modes, the presence of four prominent peaks P1 to P4 were observed and the intermediate frequency regime to degrade. A shift of the gas diffusion peak 'P1' is also observed. These shifts are associated with the EIS data quality and is an effect of trimming of the low and high frequencies during the correction process.

In the SOFC mode, the gas diffusion peak is larger compared to the SOE mode. It is also observed that peaks 'P2' and 'P3' degrade the most for RU3, while peaks 'P1' and 'P4' nearly remain constant. In the SOE mode, the DRT results from Step1 (0 hours) show

convolution of peaks ‘P3’ and ‘P4’. This observation is consistent to the result obtained in Xiufu Sun et. al. [12]. It is also observed that peak ‘P3’ degraded the most. The oxide ion transfer resistance peak ‘P4’, associated with the H2-electrode is seen at the end of the experiment. The increase in resistances of peaks P3 and P4 indicate degradation of the Ni-YSZ triple phase boundary, suggesting nickel agglomeration, oxidation or contamination.

Summary

Reversible solid oxide fuel cells are still in the development stage. Long-term stability and cyclic degradation tests are essential for better understanding of degradation mechanisms involved and to propose solutions for improving the lifetime and minimizing the risk of failures. Steady state degradation test for SOFC/SOE modes were performed on a short-stack rSOC for duration of 80/120 hours respectively at 700°C and ±0.5 A cm^{-2}. This was followed by 34/35 cyclic degradation tests with intermediate J-V and EIS measurements at ±1A DC bias with 200 mA/1000 mA perturbation in SOFC/SOE modes respectively. The total experimental duration was 1400 h. The degradation rates revealed that SOE mode degraded more than the SOFC mode. In both modes, the oxide ion transport through the H2-electrode and the O2-electrode degraded. Degradation was also found to be associated with the charge transfer process of the Ni-YSZ H2-electrode along with increase in ohmic resistance of the rSOC short stack.

Acknowledgement

This project has received funding from the European Union’s Horizon 2020 research and innovation programme under grant agreement No 731224.
Call identifier: H2020: LCE-2016-2017: LCE-33-2016.
Swiss partners are funded from the Swiss State Secretariat for Education, Research and Innovation SEFRI under contract 16. 0178, 731224

References

[1] D.R. Kothawale, J. v Revadekar, K. Rupa Kumar, Recent trends in pre-monsoon daily temperature extremes over India, Journal of Earth System Science. 119 (2010) 51–65. https://doi.org/10.1007/s12040-010-0008-7.

[2] L. v Alexander, X. Zhang, T.C. Peterson, J. Caesar, B. Gleason, A.M.G. Klein Tank, M. Haylock, D. Collins, B. Trewin, F. Rahimzadeh, A. Tagipour, K. Rupa Kumar, J. Revadekar, G. Griffiths, L. Vincent, D.B. Stephenson, J. Burn, E. Aguilar, M. Brunet, M. Taylor, M. New, P. Zhai, M. Rusticucci, J.L. Vazquez-Aguirre, Global observed changes in daily climate extremes of temperature and precipitation, Journal of Geophysical Research: Atmospheres. 111 (2006). https://doi.org/10.1029/2005JD006290.

[3] C. Zanocco, H. Boudet, R. Nilson, H. Satein, H. Whitley, J. Flora, Place, proximity, and perceived harm: extreme weather events and views about climate change, Climatic Change. 149 (2018) 349–365. https://doi.org/10.1007/s10584-018-2251-x.

[4] I.P. on C. Change, Detection and Attribution of Climate Change: from Global to Regional, in: Intergovernmental Panel on Climate Change (Ed.), Climate Change 2013 - The Physical Science Basis, Cambridge University Press, Cambridge, 2014: pp. 867–952. https://doi.org/10.1017/CBO9781107415324.022.

[5] Paris Climate Agreement, United Nations Treaty Collection. (2015). https://treaties.un.org/Pages/ViewDetails.aspx?src=TREATY&mtdsg_no=XXVII-7-d&chapter=27&lang=_en&clang=_en.

[6] D. (2016). Pauw, W.P, Cassanmagnano, D., Mbeva, K., Hein, J., Guarin, A., Brandi, C., Dzebo, A., Canales, N., Adams, K.M., Atteridge, A., Bock, T., Helms, J., Zalewski, A., Frommé. E., Lindener, A., Muhammad, Analyse and compare (Intended) National Determined Contributions, (2016). https://doi.org/10.23661/ndc_explorer_2017_2.0.

[7] D. Parra, L. Valverde, F.J. Pino, M.K. Patel, A review on the role, cost and value of hydrogen energy systems for deep decarbonisation, Renewable and Sustainable Energy Reviews. 101 (2019) 279–294. https://doi.org/https://doi.org/10.1016/j.rser.2018.11.010.

[8] G. Glenk, S. Reichelstein, Economics of converting renewable power to hydrogen, Nature Energy. 4 (2019) 216–222. https://doi.org/10.1038/s41560-019-0326-1.

[9] R. Peters, M. Frank, W. Tiedemann, I. Hoven, R. Deja, V.N. Nguyen, L. Blum, D. Stolten, Development and Testing of a 5kW-Class Reversible Solid Oxide Cell System, ECS Transactions. 91 (2019) 2495–2506. https://doi.org/10.1149/09101.2495ecst.

[10] V.N. Nguyen, Q. Fang, U. Packbier, L. Blum, Long-term tests of a Jülich planar short stack with reversible solid oxide cells in both fuel cell and electrolysis modes, International Journal of Hydrogen Energy. 38 (2013) 4281–4290. https://doi.org/10.1016/j.ijhydene.2013.01.192.

[11] M.B. Mogensen, M. Chen, H.L. Frandsen, C. Graves, J.B. Hansen, K. v. Hansen, A. Hauch, T. Jacobsen, S.H. Jensen, T.L. Skafte, X. Sun, Reversible solid-oxide cells for clean and sustainable energy, Clean Energy. 3 (2019) 175–201. https://doi.org/10.1093/ce/zkz023.

[12] X. Sun, P. v Hendriksen, M.B. Mogensen, M. Chen, Degradation in Solid Oxide Electrolysis Cells During Long Term Testing, Fuel Cells. 19 (2019) 740–747. https://doi.org/10.1002/fuce.201900081.

[13] P. Hjalmarsson, X. Sun, Y.-L. Liu, M. Chen, Durability of high performance Ni–yttria stabilized zirconia supported solid oxide electrolysis cells at high current density, Journal of Power Sources. 262 (2014) 316–322. https://doi.org/https://doi.org/10.1016/j.jpowsour.2014.03.133.

[14] P. Caliandro, A. Nakajo, S. Diethelm, J. van herle, Model-assisted identification of solid oxide cell elementary processes by electrochemical impedance spectroscopy measurements, Journal of Power Sources. 436 (2019). https://doi.org/10.1016/j.jpowsour.2019.226838.